Australian Government
Geoscience Australia

Exploring for the Future

Thermomechanical models of the Australian plate

M. Hoggard[1], J. Hazzard[2], Z. Sudholz[1,3], F. Richards[2], T. Duvernay[1], J. Austermann[4], A. L. Jaques[1], G. Yaxley[1], K. Czarnota[5] and M. Haynes[5]

[1]Australian National University, [2]Imperial College London, [3]University of Cambridge, [4]Columbia University, [5]Geoscience Australia

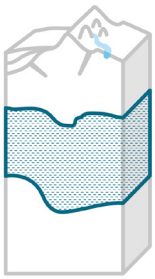

The thickness and thermal structure of continental lithosphere influences the location of seismic and volcanic hazards and is important for predicting long-term evolution of landscapes, sedimentary basins, and the distribution of natural resources. In this project, we have developed new, continental-scale models of the thermomechanical structure of the Australian plate. We begin by compiling an inventory of >15,000 geochemical analyses of peridotitic xenoliths and xenocrysts from across the continent that have been carried up to the surface in volcanic eruptions. We apply thermobarometric techniques to constrain their pressure and temperature of equilibration and perform steady-state heat flow modelling to assess the paleogeotherm beneath these sites. We subsequently use the paleogeotherms as constraints in a Bayesian calibration of anelasticity at seismic frequencies to provide a mapping between seismic velocity and temperature as a function of pressure. We apply this method to several regional-scale seismic tomography models, allowing the temperature to be continuously mapped throughout the Australian lithospheric and asthenospheric mantle. Our models include assessment of uncertainties and can be used to query thermomechanical properties, such as lithospheric thickness, heat flow through the Moho, and the Curie depth.

It is increasingly recognised that the thermomechanical properties of continental lithosphere play a fundamental role in modulating geodynamic processes across a range of spatiotemporal scales. Lithospheric thickness has been linked, for example, to seismogenic thickness and variations in the frequency and magnitude of seismicity (Craig et al., 2011), long-term active tectonics and the style of intraplate deformation (Liu and Zoback, 1997), sedimentary basin geometries (Ebinger et al., 2019), and surface heat flow (Hyndman et al., 2005). The rigid plate acts as a lid that interacts with the underlying asthenosphere, limiting the shallowest levels of decompression melting above mantle plumes and localising volcanism associated with shear-driven upwelling (Davies and Rawlinson, 2014; Duvernay et al., 2021; Niu, 2021). Thick areas of lithospheric mantle (commonly referred to as *cratons*) enhance the preservation potential of surface rocks, providing a vestige for areas of Earth's oldest continental crust (Jordan, 1978). Due to these fundamental controls on geological processes, lithospheric architecture is inexorably linked to the genesis and distribution of many natural resources, including mineral deposits (e.g. Griffin et al., 2013; Skirrow et al., 2018; Hoggard et al., 2020). Models of the lithosphere are now routinely used to underpin exploration efforts, particularly as continuous maps of thermomechanical structure allow the identification of prospective domains for resources, even in regions that are buried beneath surface cover. The general goal of this extensive collaboration has therefore been to improve these models for Australia, including increasing their resolution, reliability, and assessing their uncertainties.

Defining the lithosphere

From a compositional perspective, lithosphere comprises of two main layers – crust and mantle. Continental crust is formed from crystallised, mantle-derived melts that are buoyant and enriched in incompatible elements, including the radiogenic heat producing uranium, thorium and potassium (Jaupart and Mareschal, 2003). The lithospheric mantle is predominantly peridotitic (i.e. composed of magnesium-rich silicates) and parts of it, particularly in cratonic regions, are thought to be the residuum leftover from melt extraction early in Earth's history (Jordan, 1978). It is considerably denser than crustal rocks, but in places more buoyant and viscous than the underlying convecting mantle due to its refractory and dehydrated nature. It is also depleted in radiogenic elements and therefore has minimal internal heat production.

From a thermomechanical perspective, a vertical column through continental lithosphere is divided into three distinct domains (Turcotte and Schubert, 2002; Figure 1). First, the layer nearest to the surface, where temperatures are lowest, is known as the *mechanical boundary layer* (MBL). It consists of the crust and upper portion of lithospheric mantle. The MBL is mechanically rigid and does not actively participate in convection. Heat passing through the MBL therefore does so by conduction, with typical temperature gradients of 15–35°C/km dependent on MBL thickness and crustal radiogenic heat production. The second domain is called the *thermal boundary layer* (TBL). Due to higher temperatures, the TBL is not mechanically rigid over geological timescales and undergoes episodic destabilisation and small-scale convection. It therefore possesses a temperature profile that transitions from fully conductive in the overlying MBL to fully adiabatic in the underlying convecting mantle. The top of the convecting mantle is known as the *asthenosphere* and makes up the third domain. It is characterised by adiabatic temperature gradients of 0.4–0.6°C/km. Projecting the mantle adiabat up to the surface defines the *potential temperature*, which has a global average of ~1330°C but can locally vary by as much as ±100°C.

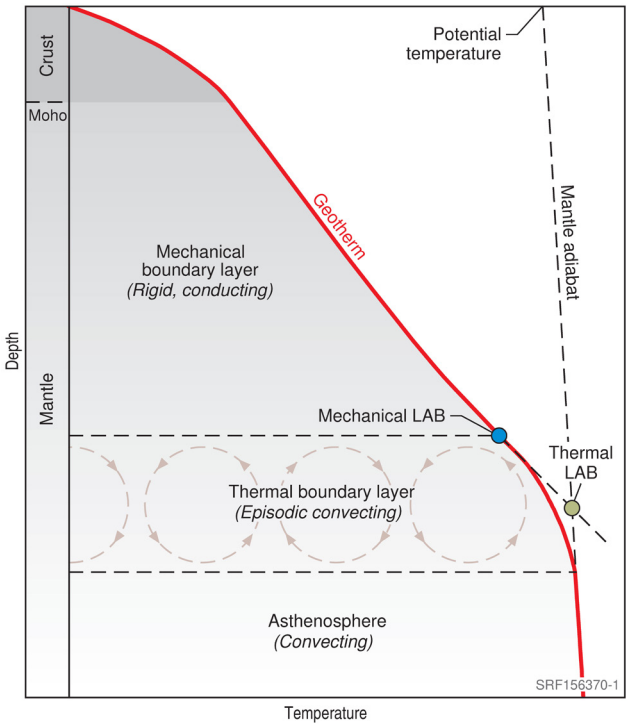

Figure 1 Schematic cartoon of the fundamental layers making up continental lithosphere. Red line = steady-state geotherm; blue and green circles = definition of mechanical and thermal lithosphere-asthenosphere boundary (LAB), respectively.

Paleogeotherm inventory

One of the strongest constraints on lithospheric structure comes from direct samples of the mantle that are brought to the surface by volcanic eruptions. Known as *xenoliths* (or *xenocrysts* if they are only single mineral grains), the petrology and geochemistry of these samples can be used to constrain the local temperature structure and lithological layering (e.g. O'Reilly and Griffin, 1985). Growing databases of such mantle xenoliths and xenocrysts (driven, in part, by exploration for diamonds) have accompanied the calibration of robust thermobarometers that exploit chemical exchanges between constituent minerals to constrain their temperature and pressure of equilibration.

Here, we have undertaken a comprehensive reassessment of xenolith and xenocryst occurrences throughout the continent. As well as digitising data from academic literature stretching back to the 1960s, we have supplemented with our own new analyses performed at the Centre for Advanced Microscopy, Australian National University (see also Sudholz et al., 2024). The final database consists of over 15,000 major and minor oxide compositions of mantle minerals, predominantly clinopyroxene and garnet, but also some orthopyroxene, olivine and spinel. These come from 60 different sites that are fairly well distributed across the continent, although central Australia is under-represented due to a scarcity of volcanic rocks hosting xenoliths in that area (Figure 2). The host volcanic rocks for mantle minerals include kimberlites and ultramafic lamprophyres in the Kimberley, Yilgarn, Gawler and North Australian Cratons, and Jurassic-to-Neogene mafic volcanics throughout the Tasmanides (stretching north-to-south across eastern Queensland, New South Wales, Victoria and into Tasmania).

We have applied published thermobarometric relationships to obtain equilibration pressure, P, and temperature, T, of mantle xenoliths and xenocrysts. Geochemical analyses were initially screened for quality using common protocols (e.g. Sudholz et al., 2023), before being assessed with two different thermobarometer pairings. For xenoliths that have analyses on co-existing clinopyroxene, orthopyroxene and garnet, we use the two-pyroxene solvus thermometer of Taylor (1998) and the garnet-orthopyroxene aluminium-exchange barometer of Nickel and Green (1985). For the single-grain clinopyroxene xenocrysts,

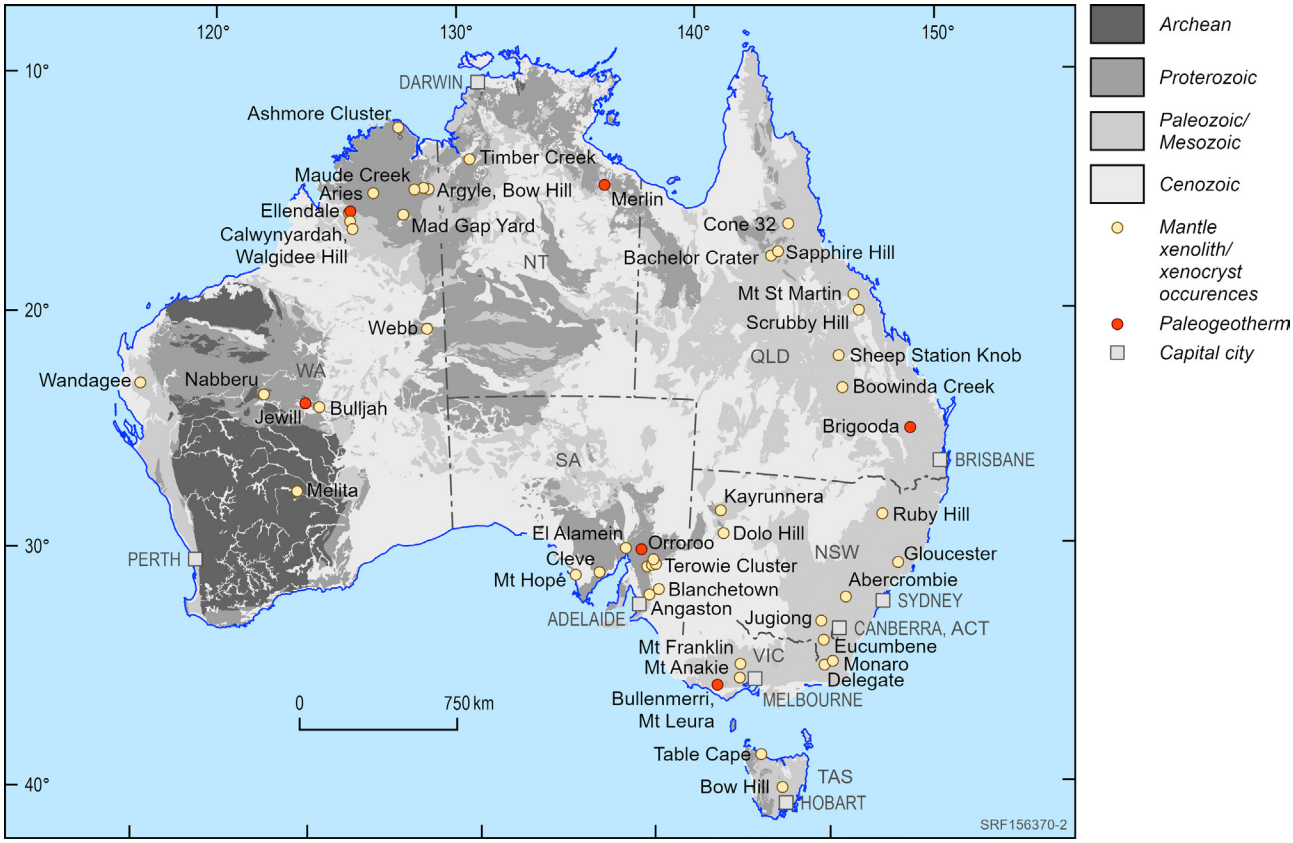

Figure 2 Localities of mantle xenolith and xenocryst occurrences compiled in this study plotted on the 1:2.5 million surface geology map (Raymond et al., 2010). Red circles correspond to six paleogeotherms shown in Figure 3.

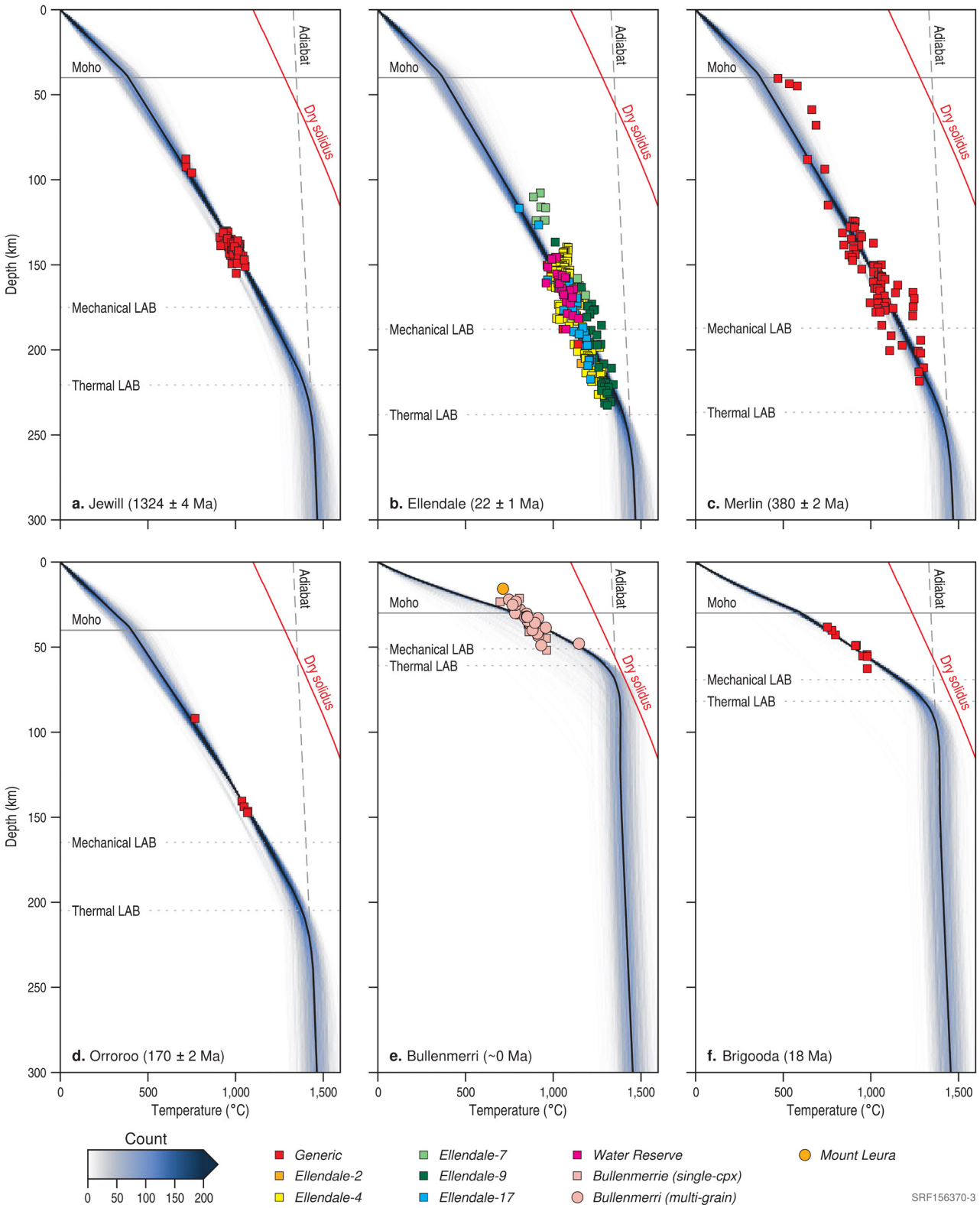

Figure 3 Representative paleogeotherms labelled with emplacement ages. Material from multiple pipes in the same vicinity have been grouped (see legend). Squares are P-T estimates obtained from single-clinopyroxene thermobarometry, circles are for multi-grain. Locations as per Figure 2.

we use the enstatite-in-clinopyroxene thermometer of Nimis and Taylor (2000) and Cr-in-clinopyroxene barometer of Sudholz et al. (2021). This thermobarometer pairing relies on the clinopyroxene having co-existed with orthopyroxene and garnet in the original peridotite assemblage. Each suite of estimated P-T points was visually inspected, and any obvious outliers culled. The values typically fall along a broadly consistent linear array, although sometimes are split into a shallower and deeper population with a conspicuous absence of diopsides from mid-lithospheric depths. Localities that are in close proximity to one another generally exhibit consistent P-T arrays and have therefore been combined into a single paleogeotherm. Examples are shown in Figure 3 and others can be found in the accompanying abstract by Sudholz et al. (2024).

Paleogeotherm modelling has been performed at each of these sites using FITPLOT by minimising misfit between each individual P-T array and a steady-state geotherm, whereby the heat flow into any point from below plus internal

radiogenic heat production is balanced by heat conducting out to shallower depths (Mather et al., 2011). Application to our dataset yields 32 usable paleogeotherms, of which we classify 27 to be of sufficiently high reliability to be of use in constructing the full thermomechanical model. We suspect that the other five are probably also reasonable but have omitted them from further use due to factors such as only returning P-T values from shallower than 30 km and/or relying on only a single P-T constraint. It is important to note that, throughout this discussion, we will primarily refer to the depth of the mechanical LAB, which is typically ~20% shallower than the thermal LAB (contra Sudholz et al., 2022, 2023a,b).

Six representative paleogeotherms are shown in Figure 3. To briefly summarise our results, the lithosphere is relatively thick beneath the Yilgarn Craton, with Melita and Jewill returning mechanical LAB depths of ~160–180 km. Northwest of the Yilgarn in the Carnarvon Basin, Wandagee returns a mechanical LAB closer to ~145 km. Webb in central Australia's Arunta province is substantially thinner, yielding ~120 km (see Sudholz et al., 2023b, for further details), while paleogeotherms from the Kimberley Craton in northern West Australia consistently infer very thick lithosphere. Data from Ashmore, Argyle, Calwynyardah, and Ellendale are all broadly consistent with the same paleogeotherm, yielding a mechanical LAB of 175–190 km. This uniformity is interesting since Argyle was emplaced at 1257 ± 15 Ma (Olierook et al., 2023), Ashmore at ~800 Ma and Calwynyardah and Ellendale date from early Miocene times (i.e. 23–17 Ma; Phillips et al., 2022). Thus, for at least a billion years, the lithosphere beneath the Kimberley Craton appears to have been relatively stable (Hoggard et al., 2020; Sudholz et al., 2023a). Continuing eastwards into the Northern Territory, Timber Creek sits on the margin of the Proterozoic Birrindudu Basin and returns a well-defined P-T array that yields a surprisingly shallow mechanical LAB of ~80 km. This depth contrasts with a value of 190 km from Merlin further east on the edge of the Proterozoic McArthur Basin. In the Gawler Craton of South Australia, Mount Hope, El Alamein and Orroroo all return consistent results and a mechanical LAB at 165–170 km depth. This inter-site agreement suggests that these paleogeotherms provide an accurate representation of lithospheric structure in the central part of Gawler Craton and that they mark the start of a gradual thinning of the lithosphere towards the east (Sudholz et al., 2022). Immediately to the east, data from the Terrowie Cluster includes a number of kimberlite fields and indicates a mechanical LAB depth of 125–135 km. Continuing eastwards across the Curnamona province and into western New South Wales, the paleogeotherms from Kayrunnera and Dolo Hill both record consistent mechanical LAB depths of 115–120 km.

Paleogeotherms from the Tasmanides are in marked contrast to everything further west, consistently indicating that the lithosphere is substantially thinner here. Starting in northern Queensland, Cone 32, Sapphire Hill and Bachelor Crater yield some of the shallowest mechanical LAB depths of 50–60 km and geotherms that make a close approach to the dry solidus in the TBL – a result that is consistent with their 1 Ma or younger emplacement ages. Scrubby Hill, Sheep Station Knob, Boowinda Creek and Brigooda have slightly deeper values (reaching ~70 km) that are broadly consistent with one another, which is encouraging given that Scrubby Hill and Boowinda Creek each rely on only a single P-T constraint. Continuing southwards over the border into New South Wales, Ruby Hill, Gloucester and Abercrombie similarly have only a few P-T data but yield mechanical LAB depths of 60 km, 70 km and 75 km, respectively, potentially hinting at gradual thickening of the lithosphere southwards. That pattern is consistent with the more extensive data from Jugiong and the Eucumbene-Tumut water tunnel (immediately northwest of the Australian Capital Territory), which indicate a mechanical LAB at 75 km. P-T constraints from Delegate and nearby Monaro are consistent with one another (although the Monaro array is less well defined) and yield ~65 km, which is interesting given the difference in their respective emplacement ages of 170 ± 5 Ma and 45 ± 11 Ma. Continuing into Victoria, both Mount Anakie and Lake Bullen Merri record thin lithosphere (mechanical LABs of 60 km and 50 km, respectively) with geotherms that approach and, in some cases, cross the dry solidus, matching expectations from their <1 Ma eruption ages. Finally, the lithosphere is slightly thicker beneath Tasmania, with Table Cape yielding a mechanical LAB at 60 km and Bow Hill closer to 70 km.

Anelastic calibration

Thermobarometric analysis of mantle xenoliths and xenocrysts provides a means of directly constraining the continental geotherm underlying the site of their eruption. These paleogeotherms are, however, sparsely distributed throughout the continent and are therefore of limited use for constraining lithospheric structure at regional scales. Seismic tomography models, on the other hand, provide laterally continuous information. Nevertheless, they provide measurements of seismic velocity, which is a derivative property of the underlying temperature structure. It is therefore necessary to convert seismic velocity variations into temperature if we are to use them to infer lithospheric structure.

The speed at which seismic energy travels through mantle rocks is strongly dependent upon their temperature. At temperatures less than 90% of the melting temperature, energy transfer occurs via minute displacements of the mineral lattice and surrounding grain boundaries that is predominantly accommodated by elastic strain. Laboratory studies have shown that the bulk and shear moduli that control this elastic deformation have an approximately linear dependence on temperature and pressure, such that seismic velocities steadily increase as the temperature reduces and/or pressure increases. Seismic velocity variations in this regime are referred to as *anharmonic*.

When temperatures rise above a threshold of 90% of the melting temperature, an additional mechanism of deformation starts to occur, known as *anelasticity* (e.g. Yamauchi and Takei, 2016). In this regime, strain of the material starts to become time-dependent in response to stress (rather than instantaneous, as in the elastic case), although it remains fully recoverable once the driving stress is removed. The effect of anelasticity is that, as temperatures continue to increase, seismic velocities drop away faster than would be expected from the anharmonic relationship. Given that temperatures within the shallow asthenosphere can come well within the 90% threshold (and indeed must cross the solidus to generate the Neogene basaltic melts found throughout much of eastern Australia), it is essential to account for anelasticity when using seismic velocity variations to construct a robust temperature model of the Australian upper mantle.

In this project, we have used the "pre-melting" YT16 anelasticity formulation of Yamauchi and Takei (2016), which contains seven material parameters that are not known a priori for the mantle. We have elected to use a recently developed Bayesian inversion scheme (Hazzard et al., 2023) to calibrate these parameters by evaluating the fit between temperatures obtained from the above paleogeotherm analysis with those derived from conversion of seismic velocity to temperature at the same localities. For the seismic tomography, we have assessed two published regional models that cover the Australian continent and include large numbers of surface waves (N.B. these waves are confined to the upper few 100 km of the Earth and are therefore excellent for imaging lithospheric structure). The first, FR12 (Fishwick and Rawlinson, 2012), used seismometers that included both permanent stations and temporary array

deployments that had been collected across the continent at that time, resulting in >13,000 individual source-to-receiver paths. Despite being over a decade old, it remains one of the higher resolution models available. The second, Aus22 (de Laat et al., 2023), is one of the most recent regional studies from the Australian plate and therefore benefits from a high level of coverage by ray paths and up-to-date techniques for inversion of seismic velocities, although selective use of available seismometers has significantly affected inferred velocity structure in some key locations, including the Kimberley Craton.

The results of our anelastic calibration of material parameters are shown in Figure 4. We focus on FR12 throughout the rest of this abstract, but equivalent results for Aus22 are also available in a supplementary dataset associated with this document. As a general rule, we find that the posterior distribution is a relatively smooth function with clear optimal anelasticity parameter values in the vicinity of the maximum a posteriori model. The two parameters that least well obey this behaviour are the diffusion creep activation energy, E_a, which shows two additional groupings at low values, and the solidus gradient, $\partial T_s/\partial z$, which returns a spread of outlier values extending above ~1.5°C/km. In terms of trade-offs, there is a distinct covariation between μ_0, $\partial\mu/\partial T$ and $\partial\mu/\partial P$. These parameters control the anharmonic velocity as a function of pressure and temperature and their trade-off has previously been recognised (Hazzard et al., 2023). The other trade-off occurs between E_a and the reference viscosity, η_r, which control the strength of the anelastic deformation process.

Final temperature model

Armed with a calibrated anelasticity parameterisation, we can convert seismic velocity variations into temperature throughout the domain of the seismic tomography model. The final processing step in our workflow is to account for the fact that these seismically inferred temperatures are not necessarily fully consistent with conductive heat flow within the MBL. For example, underestimation of crustal thickness during construction of the seismic tomography model results in artefacts related to downward bleeding of crustal velocities into the underlying mantle, which are subsequently erroneously

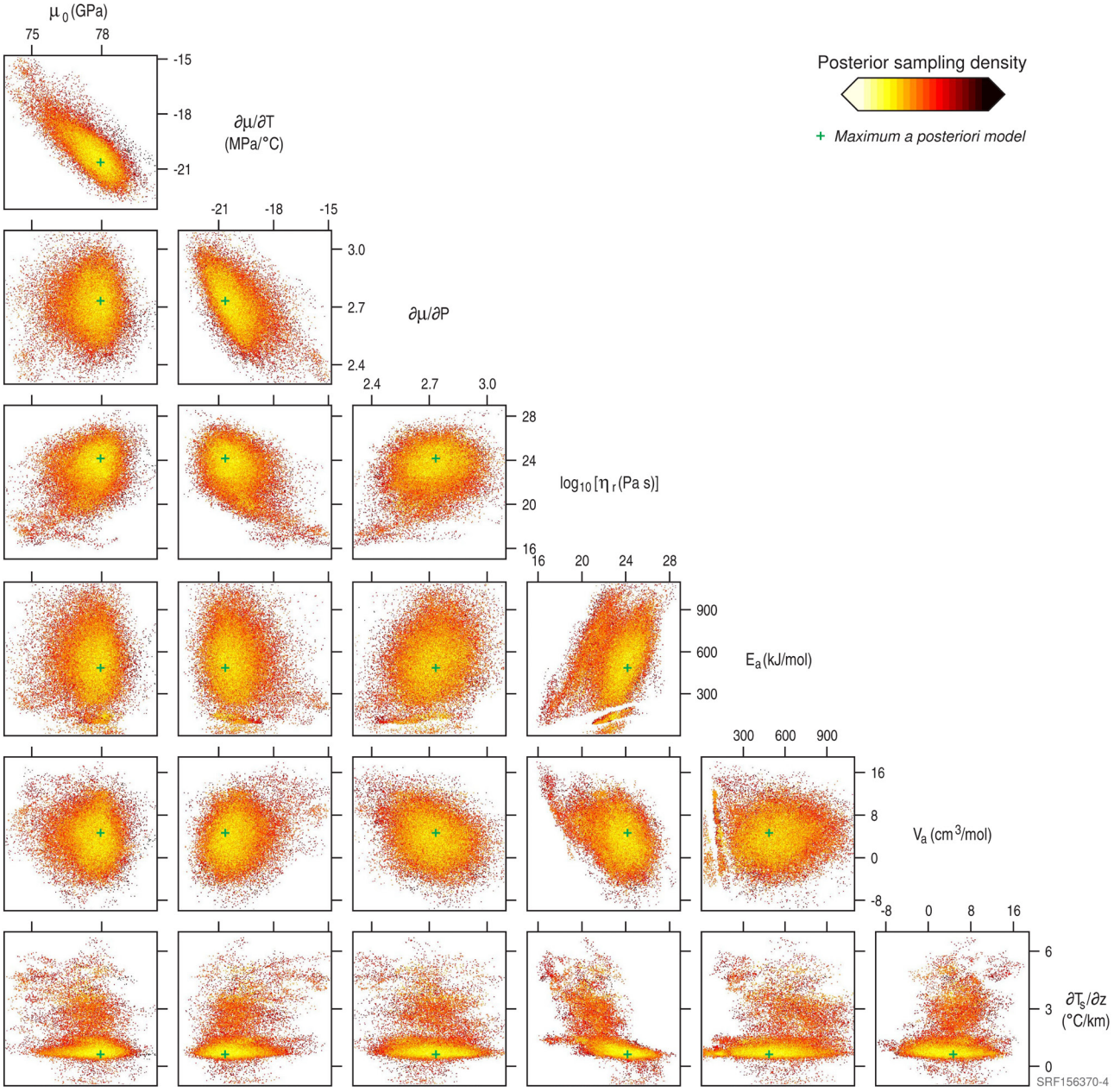

Figure 4 Posterior distributions and trade-offs between the seven calibrated anelasticity parameters for FR12 tomography model. Points = 200,000 individual samples, coloured by posterior sampling density (i.e. a measure of parameter probability); green cross = maximum a posteriori model.

converted into hot temperatures at shallow depths. We therefore fit a steady-state geotherm to the seismic-velocity-derived temperature estimates and use it to fix the temperature in regions that are affected by such anomalies. The resulting conductive temperature structure within the MBL is then smoothly blended into the original seismic velocity-derived temperatures below it. Finally, to remove any residual high-frequency noise, temperatures at each depth slice are low-pass filtered using a cosine arch with 100 km width.

The final model consists of estimates of temperature and its uncertainty as a function of location and depth throughout the Australian upper mantle. We can use the model to query a number of different properties of interest. For example, Figure 5a shows the depth to the 1175°C isothermal surface, which is a proxy for the mechanical LAB, while Figure 5b shows its uncertainty. As previously demonstrated in Hoggard et al. (2020), the major sediment-hosted base metal and Iron Oxide-Copper-Gold deposits of Australia cluster exclusively along the margins of thick lithosphere. It is important to note that the exact contour along which they reside has increased in thickness from 170 km to ~200 km in the new model – a shift that can be attributed to three factors: (i) recalibration of the Cr-in-clinopyroxene geobarometer as part of the Exploring for the Future program (which generally pushes high-pressure xenocrysts to greater depths; Sudholz et al., 2021); (ii) the greater number of paleogeotherms in our new compilation from regions of thick lithosphere (Figure 2); and (iii) improvements in our thermal-modelling workflow. Figure 5c shows the expected

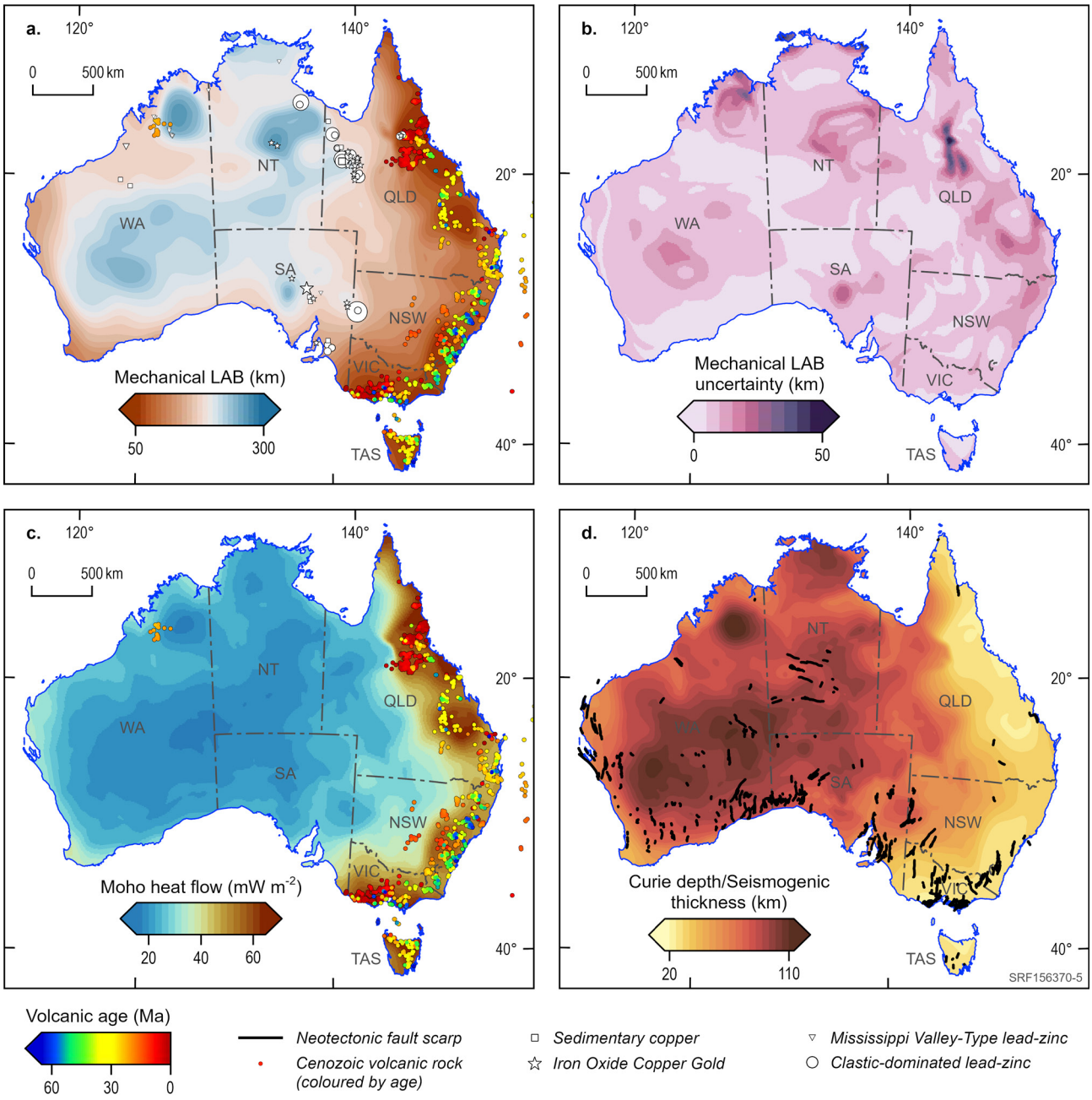

Figure 5 Outputs for the FR12-based thermal model. (a) Predicted depth of the 1175°C isotherm (proxy for mechanical LAB) for the maximum a posteriori anelasticity parameters. White symbols = major sediment-hosted base metal and IOCG deposits (symbol size scaled by total contained metal; Hoggard et al., 2020); coloured circles = locations of Cenozoic volcanism (coloured by eruption age; Ball et al., 2021; Phillips et al., 2022). (b) Uncertainty in mechanical LAB depth obtained by randomly drawing 223 sets of the a posteriori anelasticity parameters, propagating those uncertainties through the subsequent model-processing steps, and calculating two standard deviations in resulting mechanical LAB depths at every location. (c) Predicted heat flow through the Moho (as defined by AusMoho; Kennett et al., 2023) with Cenozoic volcanic rocks as before. (d) Predicted depth of the 600°C isotherm (proxy for both Curie depth and seismogenic thickness) overlain with Neotectonic fault scarps (Clark et al., 2011).

heat flow through the Moho (as defined by AusMoho; Kennett et al., 2023). Overlaying these maps with the distribution of Cenozoic volcanic rocks throughout the continent (Ball et al., 2021; Phillips et al., 2022), we can confirm that volcanism is both confined to regions of presently thin lithosphere and that the youngest volcanism in Queensland and Victoria occurs in regions with some of the highest Moho heat flow (c.f. Zielhuis & van der Hilst, 1996).

Other uses for the model include estimating the Curie depth (i.e. depth-extent of ferromagnetism), seismogenic thickness (i.e. likely maximum depth-extent of earthquakes), the contribution of temperature observed electrical conductivity anomalies obtained from magnetotelluric studies (thereby permitting isolation of residual features related to compositional variations), and 3-D mantle viscosity variations for use in viscoelastic models of surface motion and sea-level change driven by melting of ice sheets and glacial isostatic adjustment. As an example, we have plotted the depth of the 600°C isotherm in Figure 5d. This value both approximately corresponds with the Curie temperature for magnetite (although that temperature is also a function of titanium content; Lattard et al., 2006) and broadly coincides with the upper-temperature limit at which earthquakes have been observed in oceanic lithosphere (Richards et al., 2018). Thus, the model provides both a new starting estimate of Curie depth for inversions of magnetic data and a potential input into future mapping of seismogenic hazards. Indeed, when we overlay the position of neotectonic fault scarps mapped throughout the continent (Clark et al., 2011), we can see that they are generally located away from or wrap around the edges of colder, deeper areas (Figure 5d).

New tools for exploration targeting

In summary, during this project, we have developed next-generation models of the thermal structure of Australian lithosphere. These efforts have been underpinned by several key advances: (1) compilation of an extensive inventory of mantle xenolith and xenocrysts across the continent; (2) recalibration of thermobarometric relationships used to convert sample geochemistry into equilibration pressure and temperature for subsequent modelling of paleogeotherms; (3) development of a Bayesian calibration of anelasticity parameters for mapping seismic velocities into temperature in a manner that is consistent with paleogeotherms; and (4) post-processing steps to ensure that the final temperature model is consistent with the physics of conductive heat flow through the mechanical boundary layer, including an assessment of model uncertainties.

Since lithospheric architecture exerts a fundamental control on geodynamic processes, it is inexorably linked to the distribution of natural resources. Spatially continuous models, such as those developed herein, can therefore be used to identify prospective domains and expand the exploration search space, including into locations that are under cover. Development of this inversion framework renders us well-positioned to leverage insights from new tomographic models that are being produced through ongoing expansion of Australia's seismometer coverage in coming years (Gorbatov et al., 2024).

Access to Datasets

P-T estimates derived from the mantle xenocryst and xenolith compilation, paleogeotherms, and thermal models (temperature and its uncertainty, in 5 km-depth increments) obtained for the FR12 and Aus22 datasets are available as supplementary material to this abstract: https://doi.org/10.11636/149411.

Acknowledgements

Geoscience Australia acknowledges the traditional owners and custodians of Country throughout Australia and acknowledges their continuing connection to land, waters and community. We pay our respects to the people, the cultures and the elders past and present. We thank Alexei Gorbatov and Michael Doublier for providing constructive reviews.

eCat 149411 doi: https://doi.org/10.26186/149411

References

Ball P., et al., 2021. Thermal structure of eastern Australia's upper mantle and its relationship to Cenozoic volcanic activity and dynamic topography. Geophysics, Geosystems, 22:e2021GC009717. https://doi.org/10.1029/2021GC009717

Clark D., McPherson A. & Collins C.D.N., 2011. Australia's seismogenic neotectonic record: A case for heterogeneous intraplate deformation. Geoscience Australia Record 2011/11, eCat 70288. https://ecat.ga.gov.au/geonetwork/srv/api/records/a05f7892-f6f5-7506-e044-00144fdd4fa6

Craig T.J., Jackson J.A., Priestley K. & McKenzie D.P., 2011. Earthquake distribution patterns in Africa: Their relationship to variations in lithospheric and geological structure, and their rheological implications. Geophysical Journal International, 185:403–434. https://doi.org/10.1111/j.1365-246X.2011.04950.x

Davies D.R. & Rawlinson N., 2014. On the origin of recent intraplate volcanism in Australia. Geology, 42:1031–1034. https://doi.org/10.1130/G36093.1

de Laat J.I., et al., 2023. Structure and evolution of the Australian plate and underlying upper mantle from waveform tomography with massive data sets. Geophysical Journal International, 234:153–189. https://doi.org/10.1093/gji/ggad062

Duvernay T., et al., 2021. Linking intraplate volcanism to lithospheric structure and asthenospheric flow. Geochemistry, Geophysics, Geosystems, 22:e2021GC009953. https://doi.org/10.1029/2021GC009953

Ebinger C.J., et al., 2019. Kinematics of active deformation in the Malawi Rift and Rungwe Volcanic Province, Africa. Geochemistry, Geophysics, Geosystems, 20:3928–3951. https://doi.org/10.1029/2019GC008354

Fishwick S. & Rawlinson N., 2012. 3-D structure of the Australian lithosphere from evolving seismic datasets. Australian Journal of Earth Sciences, 59:809–826. https://doi.org/10.1080/08120099.2012.702319

Gorbatov A., et al., 2024. AusArray continental-scale deployment. In: Czarnota K. (ed.), Exploring for the Future: Extended Abstracts. Geoscience Australia, Canberra. https://doi.org/10.26186/149640

Griffin W.L., Begg G.C. & O'Reilly S.Y., 2013. Continental-root control on the genesis of magmatic ore deposits. Nature Geoscience, 6:905–910. https://doi.org/10.1038/ngeo1954

Hazzard J.A.N., Richards F.D., Goes S.D.B. & Roberts G.G., 2023. Probabilistic assessment of Antarctic thermomechanical structure: Impacts on ice sheet stability. Journal of Geophysical Research: Solid Earth, 128:e2023JB026653. https://doi.org/10.1029/2023JB026653

Hoggard M.J., et al., 2020. Global distribution of sediment-hosted metals controlled by craton edge stability. Nature Geoscience, 13:504–510. https://doi.org/10.1038/s41561-020-0593-2

Hyndman R.D., Currie C.A. & Mazzotti S.P., 2005. Subduction zone backarcs, mobile belts, and orogenic heat. GSA Today, 15:4–10. https://doi.org/10.1130/1052-5173(2005)015%3C4:SZBMBA%3E2.0.CO;2

Jaupart C. & Mareschal J.-C., 2003. Constraints on crustal heat production from heat flow data. In: Treatise on Geochemistry, Volume 3 (edited by R. L. Rudnick), chapter 3.02:65–84. Elsevier. https://doi.org/10.1016/B0-08-043751-6/03017-6

Jordan T.H., 1978. Composition and development of the continental tectosphere. Nature, 274:544–548. https://doi.org/10.1038/274544a0

Kennett B.L.N., et al., 2023. Refining the Moho across the Australian continent. Geophysical Journal International, 233:1863–1877. https://doi.org/10.1093/gji/ggad035

Lattard D., Engelmann R., Kontny A. & Sauerzapf U., 2006. Curie temperatures of synthetic titanomagnetites in the Fe-Ti-O system: Effects of composition, crystal chemistry, and thermomagnetic methods. Journal of Geophysical Research, 111:B12S28. https://doi.org/10.1029/2006JB004591

Liu L. & Zoback M.D., 1997. Lithospheric strength and intraplate seismicity in the New Madrid seismic zone. Tectonics, 16:585–595. https://doi.org/10.1029/97TC01467

Mather K.A., et al., 2011. Constraints on the depth and thermal history of cratonic lithosphere from peridotite xenoliths, xenocrysts and seismology. Lithos, 125:729–742. https://doi.org/10.1016/j.lithos.2011.04.003

Nickel K.G. & Green D.H., 1985. Empirical geothermobarometry for garnet peridotites and implications for the nature of the lithosphere, kimberlites and diamonds. Earth and Planetary Science Letters, 73:158–170. https://doi.org/10.1016/0012-821X(85)90043-3

Nimis P. & Taylor W.R., 2000. Single clinopyroxene thermobarometry for garnet peridotites. Part I. Calibration and testing of a Cr-in-Cpx barometer and an enstatite-in-Cpx thermometer. Contributions to Mineralogy and Petrology, 139:541–554. https://doi.org/10.1007/s004100000156

Niu Y., 2021. Lithosphere thickness controls the extent of mantle melting, depth of melt extraction and basalt compositions in all tectonic settings on Earth – A review and new perspectives. Earth-Science Reviews, 217:103614. https://doi.org/10.1016/j.earscirev.2021.103614

Olierook H.K.H., et al., 2023. Emplacement of the Argyle diamond deposit into an ancient rift zone triggered by supercontinent breakup. Nature Communications 14:5274. https://doi.org/10.1038/s41467-023-40904-8

O'Reilly S.Y. & Griffin W.L., 1985. A xenolith-derived geotherm for southeastern Australia and its geophysical implications. Tectonophysics, 111:41–63. https://doi.org/10.1016/0040-1951(85)90065-4

Phillips D., Clarke W. & Jaques A.L., 2022. Age and origin of the West Kimberley lamproites, Western Australia. Lithos, 432–433:106913. https://doi.org/10.1016/j.lithos.2022.106913

Raymond O.L., et al., 2010. Surface Geology of Australia 1:2.5 million scale dataset. Geoscience Australia. https://doi.org/10.26186/5c636e559cbe1

Richards F.D., Hoggard M.J., Cowton L.R. & White N.J., 2018. Reassessing the thermal structure of oceanic lithosphere with revised global inventories of basement depths and heat flow measurements. Journal of Geophysical Research: Solid Earth, 123:9136–9161. https://doi.org/10.1029/2018JB015998

Skirrow R.G., et al., 2018. Lithospheric architecture and mantle metasomatism linked to Iron Oxide Cu-Au ore formation: Multidisciplinary evidence from the Olympic Dam region, South Australia. Geochemistry, Geophysics, Geosystems, 19:2673–2705. https://doi.org/10.1029/2018GC007561

Sudholz Z.J., et al., 2023a. Petrology, age, and rift origin of ultramafic lamprophyres (aillikites) at Mount Webb, a new alkaline province in Central Australia. Geochemistry, Geophysics, Geosystems, 24:e2023GC011120. https://doi.org/10.1029/2023GC011120

Sudholz Z.J., et al., 2023b. Mapping the structure and metasomatic enrichment of the lithospheric mantle beneath the Kimberley Craton, Western Australia. Geochemistry, Geophysics, Geosystems, 24:e2023GC011040. https://doi.org/10.1029/2023GC011040

Sudholz Z.J., et al., 2022. Multi-stage evolution of the South Australian Craton: Petrological constraints on the architecture, lithology, and geochemistry of the lithospheric mantle. Geochemistry, Geophysics, Geosystems, 23:e2022GC010558. https://doi.org/10.1029/2022GC010558

Sudholz Z.J., Yaxley G.M., Jaques A.L. & Brey G.P., 2021. Experimental recalibration of the Cr-in-clinopyroxene geobarometer: Improved precision and reliability above 4.5 GPa. Contributions to Mineralogy and Petrology, 176:11. https://doi.org/10.1007/s00410-020-01768-z

Sudholz Z.J., et al., 2024. Xenolith constraints on lithospheric architecture and mantle geochemistry of Australia. In: Czarnota K. (ed.), Exploring for the Future Extended Abstracts, Geoscience Australia, Canberra. https://doi.org/10.26186/149242

Taylor W.R., 1998. An experimental test of some geothermometer and geobarometer formulations for upper mantle peridotites with application to the thermobarometry of fertile lherzolite and garnet websterite. Neues Jahrbuch für Mineralogie - Abhandlungen, 172:381–408. https://doi.org/10.1127/njma/172/1998/381

Turcotte D.L. & Schubert G., 2002. Geodynamics. Cambridge University Press, Cambridge, 2nd edn.

Yamauchi H. & Takei Y., 2016. Polycrystal anelasticity at near-solidus temperatures. Journal of Geophysical Research: Solid Earth, 121:7790–7820. https://doi.org/10.1002/2016JB013316

Zielhuis A. & van der Hilst R.D., 1996. Upper-mantle shear velocity beneath eastern Australia from inversion of waveforms from SKIPPY portable arrays. Geophysical Journal International, 127:1–16. https://doi.org/10.1111/j.1365-246X.1996.tb01530.x

GA SRF162988